Journal of the Brazilian Society of Mechanical Sciences and Engineering (2020) 42:590
https://doi.org/10.1007/s40430-020-02668-w

TECHNICAL PAPER

Thermal performance optimization of heat pipe using nanofluid: response surface methodology

Naveen Kumar Gupta[1] · Abhishek Sharma[2] · Pushpendra Kumar Singh Rathore[3] · Sujit Kumar Verma[1]

Received: 6 February 2020 / Accepted: 21 September 2020

Abstract

Nanofluids are the new class of thermo-fluidics. Researchers found that nanofluids have the potential to enhance the thermal performance of various thermal applications. In the present paper, parametric optimization of the thermal performance of nanofluid-filled heat pipe is performed using response surface methodology. The operating parameters like power input, inclination angle, filling ratio of nanofluid (working fluid) and nanofluid concentration are considered. Optimization study predicted the optimum value of thermal efficiency, thermal resistance and wall temperatures as 66.40%, 0.3884 °C/W and 78.86 °C, respectively, at 112 W power input, 55% filling ratio, 1.1% nanofluid concentration and at 58.5° inclination angle. The predicted and experimental optimization results are in good agreement.

Keywords Thermosyphon · Nanofluids · Thermal performance · Response surface method

Abbreviations

NF	Nanofluid
TR	Thermal resistance
CCRD	Central composite rotating design
HP	Heat pipe
RSM	Response surface methodology
W	Watt
TR	Thermal resistance (°C/W)

List of symbols

T	Wall temperature in °C
Q and ΔQ	Heat supplied and uncertainty in heat supplied
I and ΔI	Current supply and uncertainty in the current supply
q and Δq	Heat flux and uncertainty in heat flux
l_e	Length of the evaporator section
l_a	Length of adiabatic section
A_{cs}	Cross-sectional (inner) area of the heat pipe
R	The thermal resistance of heat pipe
a	Inclination angle (°)
p	Input power (watt)
V and ΔV	Voltage and uncertainty in voltage
A and ΔA	Surface area and uncertainty in surface area
ΔT and $\Delta(\Delta T)$	The temperature difference of evaporator and condenser section and their uncertainty
l_c	Length of the condenser section
K_{eff}	Effective thermal conductivity of the heat pipe
L_{eff}	The effective length of the heat pipe
r	Filling ratio (%)
c	Concentration of nanofluid (vol%)

1 Introduction

Heat exchangers are the inevitable process equipment used in various thermal applications. Heat pipe (HP) is a special category of heat exchangers. Figure 1 shows the working of the mesh wick heat pipe. It works on phase change closed-cycle phenomenon. Thermal performance of heat pipe (TPHP) depends upon the thermophysical properties of working fluids. All liquids (except liquid metal) have poor

Technical Editor: Francis HR Franca, Ph.D.

✉ Naveen Kumar Gupta
naveen_glau@yahoo.in; naveen.gupta@gla.ac.in

[1] Department of Mechanical Engineering, Institute of Engineering and Technology, GLA University, Mathura, India

[2] Department of Mechanical Engineering, GL Bajaj Institute of Technology and Management, Greater Noida, India

[3] Department of Mechanical Engineering, Indian Institute of Technology (BHU) Varanasi, Varanasi, India

Published online: 21 October 2020

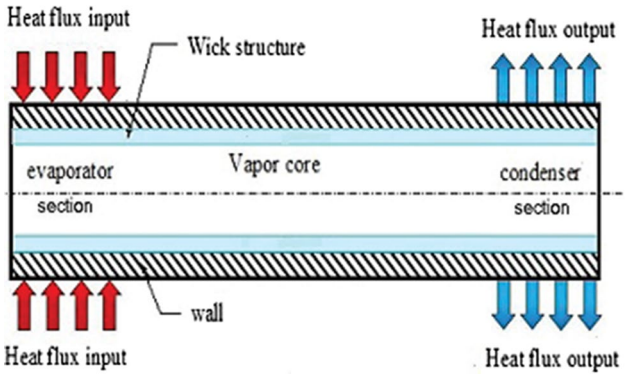

Fig. 1 Working principle of heat pipe [14]

thermal conductivity. All possible methods to increase the heat transfer like creating turbulence, increasing area etc. are restricted by the poor thermal conductivity of liquids. Researchers noticed that nanofluids are the new generation of thermal fluids. In 1995, Choi et al. [1] introduced nanofluids as the most promising thermal fluids for future endeavours. Nanofluids are the suspension of nanoparticles (size < 100 nm) in base fluids.

Generally, nanoparticles having high thermal diffusivity are considered for nanofluid (NF) preparation [2]. Researchers dispersed nanoparticles in phases change materials also to increase their thermal conductivity [3, 4]. Researchers prepared NFs by stirring the nanoparticles of various metals, metal oxides, carbides, nitrides and different types of carbon with base fluids like water, alcohols and different oils etc. Researchers examined the thermophysical property of NFs with a wide range of concentration and temperatures. Das et al. [5] presented an experimental investigation regarding the increase in thermal conductivity of NFs like Al_2O_3/H_2O and CuO/H_2O with the increase in temperature and concentration. Authors concluded that the enhancement of thermal conductivity shows a dramatic increase with temperature. The rate of increment depends on the concentration of nanoparticles also. Trisaksri et al. [6] reviewed the heat transfer characteristics of NFs. Authors concluded that the enhancement in thermal conductivity of NFs depends on particles concentration, shape, size and type etc. It also depends on the type of base fluid, pH value of NF and type of particle coating. Heat transfer performance increases with the increase in particles concentration (for same Reynolds number). At high heat flux, experimental results revealed that nanoparticles addition did not increase the heat transfer performance in pool boiling processes but critical heat flux was increased significantly. Therefore, NFs may be used for cooling in high heat flux applications. Gupta et al. [7] reviewed the thermophysical properties of NFs. Authors discussed the effect of nanoparticles concentration and temperature on thermal conductivity, specific heat and viscosity of NFs. The other influencing parameters are nanoparticles shape, size, material type, sonication time, base fluids and characteristics of interfacial layer etc.

Many research articles regarding the thermophysical properties of NFs have been published in the last 20 years. Researchers [8–11] concluded that NFs show superior thermophysical properties. Therefore, NFs may be considered as effective working fluids for heat transfer applications. Researchers used NFs in various heat exchangers and noticed higher thermal performance as compared to the base fluids.

Research on NFs application in HPs has been carried out mainly in three directions. The first direction is the experimental studies, showing the enhancement/deterioration in thermal performance of HP. Majority of research articles showed the enhancement in thermal performance. Some researchers analysed the mechanisms responsible for the above change. Mahdavi et al. [12] investigated the thermal performance of a heat pipe. Authors investigated the effect of input power, orientation and volume of working fluid on the thermal performance of HP. A previously developed numerical model was validated using experimental data. Authors noticed a good agreement between experimental and numerical results. Gupta et al. [13] reviewed the various mechanisms responsible for the change in heat transfer performance of HP and found that the enhanced thermal conductivity, increased wettability, Brownian motion of nanoparticles and reduction in bubble formation (suspended nanoparticles puncture the bubbles generated at the solid–liquid interface) are the major causes. Other causes are enhancement in convective heat transfer coefficient, enhancement in surface area in the evaporator by the accumulation of nanoparticles.

Researchers used various NFs as working fluids in HPs and noticed a reduction in wall temperatures and thermal resistance. Gupta et al. [14] investigated the thermal performance using CuO/H_2O NF as working fluid. Authors noticed 20.5% reduction in thermal resistance and 15.3% enhancement in thermal efficiency as compared to water. Buschmann [15] published a review article on the NFs application in thermosyphon and heat pipe. The author concluded that NFs are promising working fluids. The thermal resistance of thermosyphon, HPs and oscillating HPs using nanofluid as working fluids reduced significantly. Although many questions regarding nanofluid characteristics, mechanisms and optimization are still open. In the last 2 decades, more than hundreds of research papers on thermal performance of HP using nanofluids have been published. Researchers noticed the significant enhancement in thermal performance. They generally claimed that the enhancement is due to the increase in thermal conductivity, enhanced surface area, bombardment of the bubbles by nanoparticles, increase in wettability etc. Gupta et al. [16] investigated the thermal

performance of HP using water as working fluid. Authors investigated the effect of operating parameters like the volume of the working fluid, power supply and inclination angle on thermal performance. Authors noticed that the increase in the volume of working fluid and power supply increases the thermal performance of HP. The orientation up to a certain value increases the thermal performance of HP after that it decreases. The most favourable angle depends on the viscosity, surface tension and wettability of the contact surface. Gupta et al. [17, 18] noticed that NF-filled heat pipe shows higher thermal performance as compared to a water-filled HP. But in prolonged working condition, due to sedimentation and agglomeration of nanoparticles, the thermophysical properties of NFs deteriorated. The deterioration in thermophysical properties causes a decrease in thermal performance also.

In the present scenario, good numbers of research papers are available on NF application in the heat pipe. Majority of the research outcomes support that the NF may be an effective working fluid for heat pipe. In some cases, nanofluids suppress the thermal performance of HP. Therefore, researchers have their different opinion regarding NFs application. Many questions regarding their mechanisms are still open for further investigations. Therefore, more experimental studies are required to draw some firm conclusions and to explore the hidden causes.

Second research direction is the numerical investigations. Researchers considered the various models to find out the thermophysical properties of NFs like thermal conductivity, viscosity and density. Gupta et al. [19] performed a numerical investigation on CeO_2/H_2O NF application in HP. Authors noticed a good agreement in wall temperatures obtained through numerical and experimental study. Poplaski et al. [20] performed a numerical simulation to investigate the effects of NFs like Al_2O_3, CuO and TiO_2 in the heat pipe. Authors also performed parametric study through experimentation and found good agreements between numerical and experimental results. Authors concluded that the increase in the concentration of NF after certain limit reduced the convection currents in mesh wick of the HP. The reduction in convection current leads to the reduction in heat transfer capacity of the HP. Solomon et al. [21] performed a numerical study using Cu/H_2O NF in a mesh wick HP. Authors solved mass, momentum and energy equation for vapour and liquid region. It was noticed that the addition of nanoparticles reduced wall temperature, thermal resistance, vapour temperature and operating pressure. Huminic et al. [22] investigated numerically (three-dimensional analysis) the heat transfer performance of thermosyphon HP using water and water-based iron oxide NFs. Researchers examined the wall temperature distribution, heat transfer coefficient and thermal resistance. Numerical results were in good agreement with the theoretical model and experimental data. Many other numerical studies [23–25] were performed. Researchers concluded that NFs are more efficient working fluid as compared to base fluids.

Third research direction is the parametric optimization of HP using NFs. In the open literature, limited research studies on parametric optimization of HP using NFs are available. Parametric optimization of thermal performance is the next level of investigation. Therefore, in the present work authors attempted to optimize the thermal performance of CuO/H_2O nanofluid-filled HP using response surface methodology (RSM). Authors also highlighted the mechanisms responsible for the change in thermal performance.

2 Methods and materials

2.1 Preparation and characterization of nanofluid

In the present study, CuO nanoparticles are purchased from Alfa-Essar (USA). The weighted nanoparticles were dispersed into water to prepare CuO/Water NF. The mixture was sonicated for 6 h for good stability. The nanoparticles were in the range of 30–50 nm (Table 1).

In present work, degassed and distilled water was used. Double distillation unit (double distillation process) was used to prepare the water. Vacuum degasser was used to degas the distilled water and nanofluids before charging the heat pipe. After each experiment, remaining non-condensable gases were also removed with the help of a vacuum pump. NFs of vol% 0.5, 1.0 and 1.5 have been prepared by two-step method. Sedimentation test has been done to ensure the stability of NF. Samples of NFs were kept for 2 weeks. After 2 weeks, no sedimentation or agglomeration was observed.

2.2 Experimental setup

In the present work, authors investigated the thermal performance of heat pipe using CuO/H_2O NF. Figures 2 and 3 show the actual view and schematic view of set up,

Table 1 Nanoparticles details

S. no	CuO nanoparticles	Description
1	Colour	White powder
2	Density	6.31 g/cm^3
3	Thermal conductivity	33 W/m K
4	Particle size	30–50 nm
5	Purity (%)	≥ 99.9
6	Specific surface area	200–220 m^2/g
7	Morphology	Spherical
8	Atomic weight	79.545 g/mol

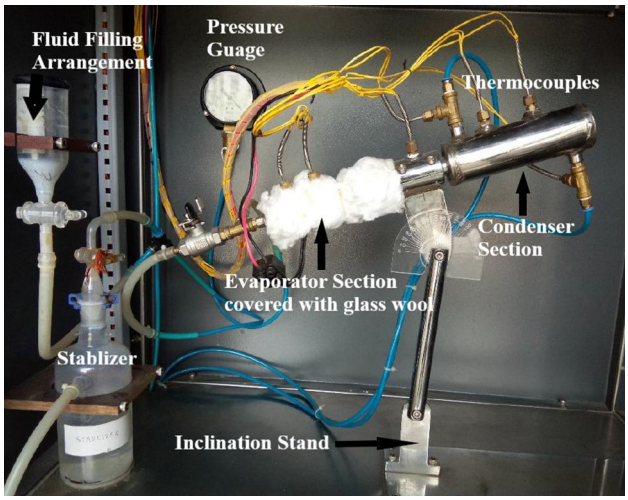

Fig. 2 Photographic view of the experimental setup [14]

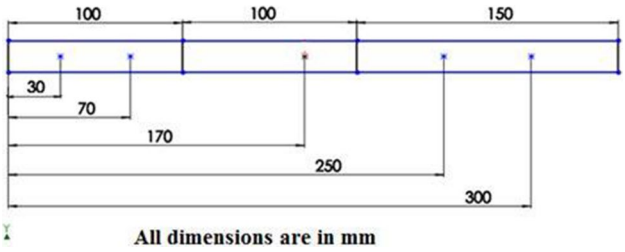

Fig. 4 Locations of all thermocouples on the heat pipe

respectively. Heat is supplied through the evaporator section using 500 W (circumferential type) electric heater. Control switch of the heater is used to vary the input power.

In present work, constant temperature water cooling bath system is used to release the heat transfer through the condenser section. K-type thermocouples are mounted on the surface of HP to measure the wall temperatures of all the three sections. Locations of all the thermocouples are represented in Fig. 4. At evaporator Sect. 4, thermocouples (2 at the outer surface and 2 at inner wall surface) are mounted. Similarly, at adiabatic and condenser section one–one and two–two thermocouples are attached to outer-inner surface, respectively. All the thermocouples are attached to a data acquisition system for temperature recording purpose. A vacuum pump is used to maintain 10–15 kPa vacuum pressure inside the HP. A charging arrangement is used to fill the different working fluid. Filling ratio is considered in the present investigation. The filling ratio is defined as the ratio of the volume of working fluid to the volume of the evaporator section. A stabilizer is used to maintain a constant vacuum pressure inside the HP. Proper insulation is provided on the outer surface of the wall.

Two thermocouples are mounted on the outer surface of the insulation, to measure the heat loss from the HP. At condenser side, the temperature of inlet and outlet water was measured by T-type thermocouples. In the present work, analysis has been done in steady-state. Therefore, temperatures have been considered after the set attains the steady-state. The input power supply, filling ratio, concentration of NF and orientation of HP are the input parameters. Wall temperatures, thermal resistance and thermal efficiency are the output parameters. The detail of HP and the uncertainties in measurements of different parameters are shown in Tables 2 and 3, respectively.

Cleaning of heat pipe consists of two steps: degreasing and deoxidization.

Degreasing:

- The wire mesh, end caps and inner surface of the tube were first cleaned with a soft bristle brush.
- Rinsed in clean distilled water.

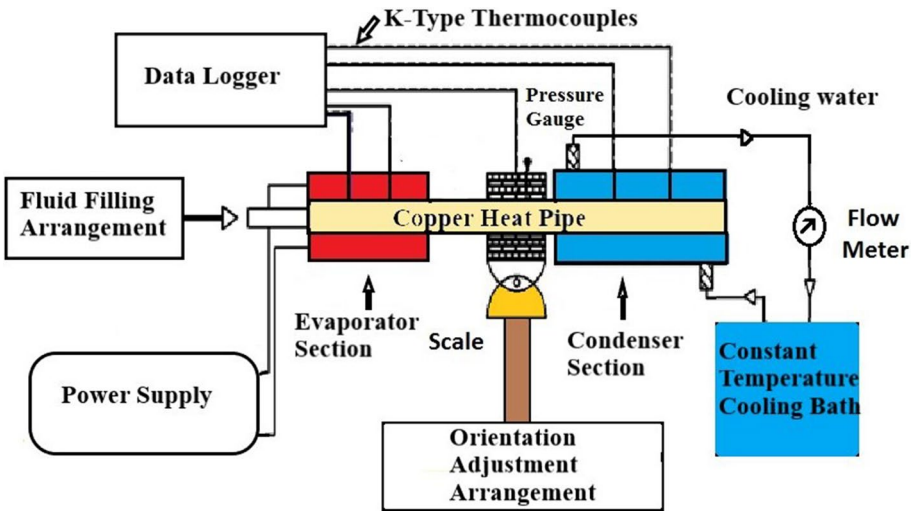

Fig. 3 Schematic of the experimental setup [14]

Table 2 Design parameters of the heat pipe

s. no	Name	Dimension (mm)/material
1	Heat pipe material	Copper
2	Length of the heat pipe	450
3	Outer diameter	24
4	Inner diameter	22.6
5	Evaporator length	150
6	Adiabatic length	100
7	Condenser length	200
8	Wick material	Stainless steel (SS304)
9	Wick type	Screen wire mesh
10	Mesh per inch	50
11	Number of strands/inch	210
12	Number of multiple layers of similar screen mesh	3
13	Porosity	0.64
14	Permeability, K (m^2)	1.8×10^{-10}
15	Wire diameter (mm)	0.041
16	Aspect ratio (AR)	1
17	Aperture size per linear inch	17.18
18	Percent open area (POA)	45.65%
19	Wick crimping factor	1.04
20	Thermocouples	10 K-type and 2 T-type

Table 3 Uncertainties in different measurements

S. no	Parameters	Uncertainties
1	Pressure	0.51%
2	Temperature	0.9 °C
3	Water flow rate	0.82%
4	Current	0.21%
5	Voltage	0.69%

- After that, all the parts were soaked in a solution of 10% sulphuric acid for 30 s.
- Again rinsed with clean water.
- Finally all parts were immersed in a methanol solution to remove any trace of water.

After these degreasing steps, deoxidization was conducted.

- Screen mesh was immersed for 30 s in a liquid deoxidizer that consisted of a combination of sodium dichromate (44 g/L), 7% by volume sulphuric acid and water.
- Finally, all parts were rinsed in clean distilled water for several minutes.
- All parts were immersed in the methanol solution.

After wick installation, final cleaning was conducted using 10% by volume sulphuric acid and rinsing in clean distilled water for several minutes.

During the fabrication of the heat pipe experimental set up, there was an extra piece of copper pipe. Therefore, a copper substrate was prepared. The surface roughness of the substrate was measured by a laser profilometer and found to be $R_a = 0.22$ µm, $R_z = 1.82$ µm and $R_q = 0.28$. The substrate was boiled with nanofluid for 1.5 h. After boiling, surface roughness was again measured and found the higher value of surface roughness ($R_a = 0.25$ µm, $R_z = 1.91$ µm, and $R_q = 0.35$). The surface roughness was increased due to the deposition of nanoparticles on the surface. Due to the presence of nanoparticles layer, wettability increases which in turn increase the critical heat flux and finally enhanced the thermal performance of the HP [26].

2.3 Uncertainty analysis

In experimental work, uncertainty analysis is an inevitable step. Moffat [27] presented the method of describing the uncertainty in the experimental study. The uncertainties in the measurement of heat input, heat flux and thermal resistance are calculated as [28]

$$\frac{\Delta Q}{Q} = \left[\left(\frac{\Delta V}{V}\right)^2 + \left(\frac{\Delta I}{I}\right)^2\right]^{1/2} \tag{1}$$

$$\frac{\Delta q}{q} = \left[\left(\frac{\Delta Q}{Q}\right)^2 + \left(\frac{\Delta A}{A}\right)^2\right]^{1/2} \tag{2}$$

$$\frac{\Delta R}{R} = \left[\left(\frac{\Delta Q}{Q}\right)^2 + \left(\frac{\Delta(\Delta T)}{\Delta T}\right)^2\right]^{1/2} \tag{3}$$

The uncertainty associated with the heating area was calculated and found to be approximately 1.2%. The uncertainty in the heat loss was 5.4%. The maximum uncertainty in heat supplied, heat flux and thermal resistance were 3.4%, 4.9% and 6.8%, respectively. Similarly, uncertainty associated with filling ratio was 3.5% approximately.

2.4 Governing equations

Suppose, T_{Eo} and T_{co} are the average wall temperatures of the outer surface of the evaporator and condenser section, respectively. Similarly, T_{Ei} and T_{ci} are the average wall temperatures of the inner surface of the evaporator and condenser section, respectively.

There are two thermocouples (K-type) attached to the outer surface and two thermocouples (K-type) attached at the inner surface of the evaporator to measure the temperatures. Similarly, there are two thermocouples (K-type) attached to the outer surface and two thermocouples (K-type) attached at the inner surface of the condenser section to measure the temperatures. The thermal resistance of the evaporator section (R_E) is defined as the ratio of temperature difference of outside and inside wall surface of the evaporator section (ΔT_E) to the heat supplied (Q_{in}). Therefore, $\Delta T_E = T_{Eo} - T_{Ei}$.

The thermal resistances of the evaporator section is calculated as [29]:

$$R_E = \frac{\Delta T_E}{Q_{in}} \tag{4}$$

Similarly, the thermal resistance of the condenser section (R_C) is defined as the ratio of temperature difference of outside and inside wall surface temperature (ΔT_C) to the heat rejected through the condenser section (Q_{out}).

Therefore, $\Delta T_C = T_{co} - T_{ci}$.

The thermal resistances of the condenser section are calculated as [29]:

$$R_C = \frac{\Delta T_C}{Q_{out}} \tag{5}$$

The total thermal resistance of HP is calculated as

$$R = (T_{Eo} - T_{co})/Q_{out} \tag{6}$$

Convective heat transfer coefficients of the evaporator (h_e) and condenser (h_c) sections are calculated as:

$$h_e = \frac{Q_{in}}{\pi d l_e (T_{E,i} - T_{sat})} \tag{7}$$

$$h_c = \frac{Q_c}{\pi d l_c (T_{sat} - T_{c,i})} \tag{8}$$

The effective thermal conductivity (K_{eff}) of HP is expressed as:

$$K_{eff} = L_{eff}/(A_{cs}R) \tag{9}$$

$$L_{eff} = L_e/2 + L_a + L_c/2 \tag{10}$$

Thermal efficiency is the performance index of the HP. It is defined as the ratio of heat transferred through the condenser section to the heat supplied to the evaporator section of HP. Thermal efficiency (η) can be determined as:

$$\eta = \frac{MC(T_2 - T_1)}{Q_{in}} \tag{11}$$

where M is the mass flow rate of cooling water, C is the specific heat of water and $(T_2 - T_1)$ is the temperature difference of outlet and inlet cooling water, where heat is supplied to the evaporator section $(Q_{in}) = VI$.

2.5 Experimentation

Experiments were performed to examine the heat transfer performance of NFs concerning the base fluid (distilled water). The thermal efficiency of HP using distilled water and NFs as working fluids was investigated. The filling ratio was taken as 50%. The orientation of the HP was horizontal (Inclination angle = 0°). Figure 5 shows the variation in the thermal efficiency of HP with power and concentration of nanofluids.

Figure 5 shows that NF-filled heat pipe shows higher thermal efficiency as compared to water. Among all the concentration (0–1.5%), 1.0% NF-filled heat pipe shows 13.16% higher thermal efficiency as compared to water. Figure 6 shows the variation of thermal resistance with power for different working fluids.

Figure 7 shows that the effect of nanoparticles deposition reduces the thermal resistance of heat pipe using pure water as working fluid. In the present experimental investigation, four measurements have been taken for each experiment and their standard deviation has been considered as error margin.

Authors used distilled water as working fluid and noticed that the thermal resistance increases with the increase in negative angle (Fig. 8). Heat pipe experimental set up works well for all negative angles (0°,15°,30°,45°,60°,75° and 90°).

Figure 9 shows the variation in thermal resistance of HP with power for different gravity-assisted inclination angles using D.I water as working fluid. Thermal resistance

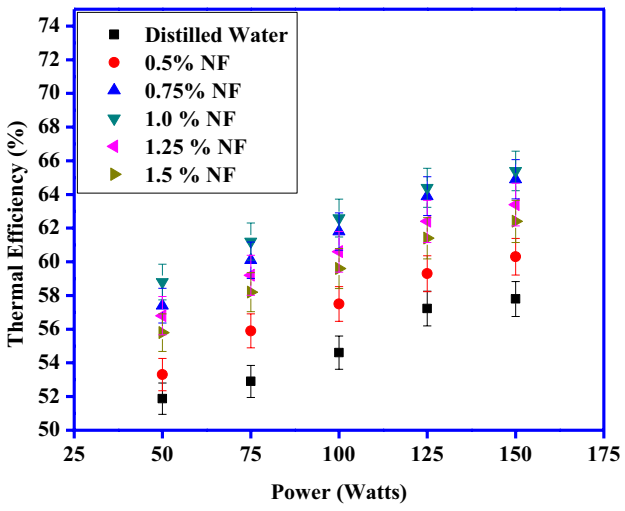

Fig. 5 Variation in thermal efficiency with power and concentration of nanofluids

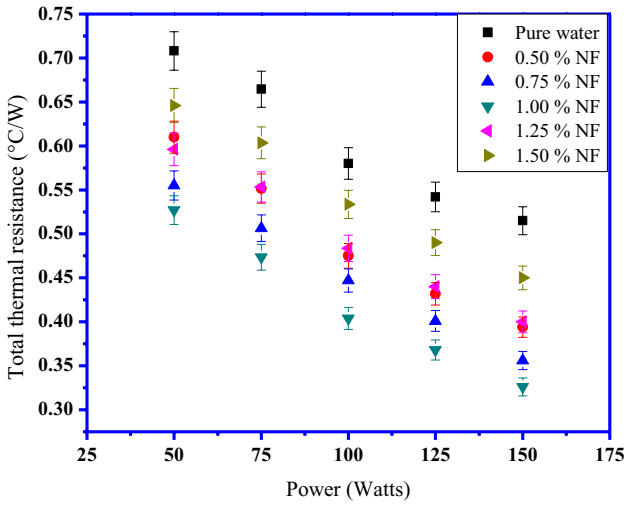

Fig. 6 Variation of total thermal resistance with power for CuO/H_2O nanofluids

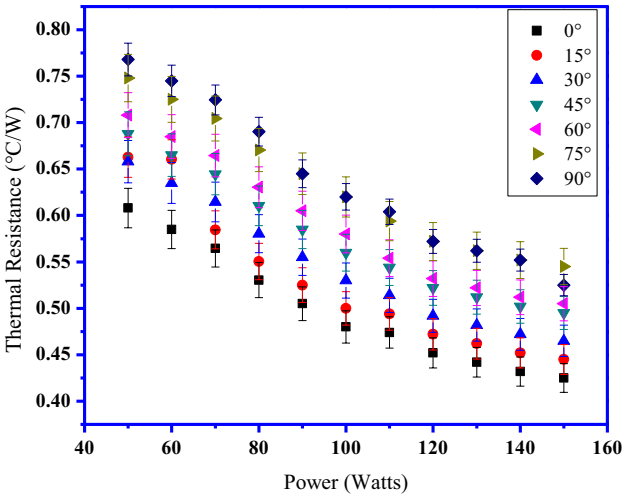

Fig. 8 Variation in thermal resistance of HP with power for gravity opposed angles using distilled water

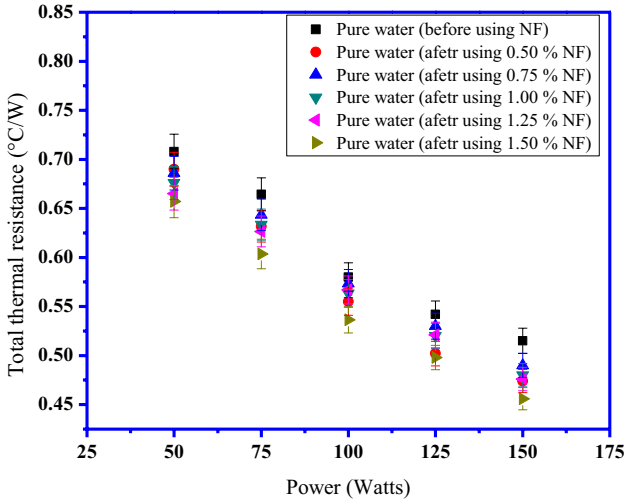

Fig. 7 Variation of total thermal resistance with power for pure water

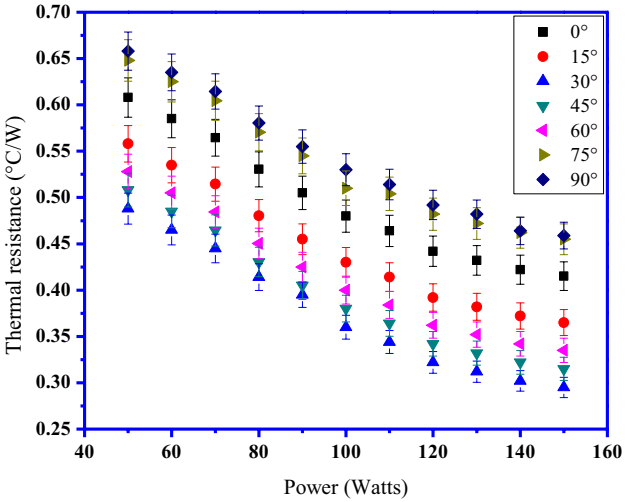

Fig. 9 Variation in thermal resistance of HP for gravity-assisted angles using distilled water

decreases up to 30° and beyond that, it increases. The existence of inclination angle corresponding to minimum thermal resistance (or maximum thermal performance) is decided by gravity force, flow resistance and capillary effect etc.

2.6 RSM methodology

RSM methodology is used to find the optimum solution. It is used to access the best structure of the input variables for achieving the highest results with the least number of tests. This technique can be utilized in certain fields and does not have any constraint-based on its application.

In this work, RSM architecture that can suitable the central composite rotating design (CCRD) matrix, which has five stages concerning the individual factors. The most fruitful and best among architecture available in the middle composite rotating architecture which is adapted by adding two laboratory experiment level along with each coordinate axis at the opposite direction of the origin and a distance same to the semi-diagonal of the hypercube of the factorial architecture and new extreme values (low and high) for each factor added in this architecture. In this work, input power, inclination angle, filling ratio and concentration of NF were considered as an input variable and potentially affect the system responses. The system responses considered are wall temperature, thermal resistance and thermal efficiency. System range of inputs with different levels is mentioned in

Table 4. Experimental results obtained after implementing the CCRD are stated in Table 5.

After the experimentation, as per the architecture matrix, ANOVA was applied, which offers quantitative results about the *p* value. The *p* value is explained as the alternative to the rejection levels to provide the lowest level of worth at which the null hypothesis would be rejected. The highest level of *p* is taken as 0.05 and the values above than 0.05 are referred to as irrelevant.

To ensure RSM feasibility of the developed model, the *S* value was obtained for wall temperature, thermal resistance and thermal efficiency which are 0.726, 0.426 and 4.991, respectively. R^2 value are 95.11%, 96.93% and 95.29%, respectively, R^2 (adj) values are 92.9%, 96.48% and 96.9%. The "R^2 value" is satisfactory as it was above 95% for the samples.

S Value represents the average distance that the observed values fall from the regression line. Smaller values indicate that the observations are closer to the fitted line. R^2 evaluates the scatter of the data points around the fitted regression line. R^2 value can be given by the percentage of the dependent variable; higher R^2 values indicate the feasibility of data analysis.

Table 4 Coded stages

System inputs	Coded stages				
	−2	−1	0	1	2
Power input (W)	50	75	100	125	150
Inclination angle (θ)	30	45	60	75	90
Filling ratio (%)	30	40	50	60	70
Nanofluid concentration (wt%)	0.5	0.75	1.0	1.25	1.5

Table 5 Experimental design matrix

S. no	Power (W)	Angle (θ)	Filling ratio (%)	Concentration (%)	Temp. (°C)	TR (°C/W)	TE (%)
1	125	75	60	1.25	81.5	0.515	66.5
2	100	60	50	1.0	78	0.4	65
3	100	60	50	1.0	78	0.4	65
4	100	60	70	1.0	75	0.47	62
5	125	45	60	0.75	82.5	0.515	64
6	75	45	60	0.75	75.5	0.63	60
7	125	75	60	0.75	83	0.555	63.5
8	75	45	40	1.25	79.5	0.58	62
9	75	45	60	0.75	75.5	0.62	60
10	100	60	50	0.50	81	0.5	61.2
11	100	60	50	1.0	78	0.4	65
12	100	60	30	1.0	82	0.45	60
13	75	75	40	1.25	80	0.61	61.5
14	100	60	50	1.0	78	0.4	65
15	100	60	50	1.5	82	0.45	64
16	125	75	40	0.75	87.5	0.57	62.5
17	75	75	60	1.25	77	0.59	62.5
18	50	60	50	1.0	72	0.58	60
19	75	75	60	0.75	76	0.64	59
20	100	30	50	1.0	81	0.52	63
21	100	90	50	1.0	80	0.6	60
22	75	45	60	1.25	76	0.6	63
23	100	60	50	1.0	78	0.4	65
24	100	60	50	1.0	78	0.4	65
25	125	45	40	1.25	86.5	0.475	66
26	125	75	40	1.25	87	0.5	65.5
27	125	45	60	1.25	83	0.485	67
28	75	75	40	0.75	79.5	0.64	58.5
29	100	60	50	1.0	78	0.4	65
30	125	45	40	0.75	86	0.55	63
31	150	60	50	1.0	83	0.378	69

3 Discussion on findings

MINITAB17 software was used to obtain the surface and contour plots. In the present study, four input parameters like power input, inclination angle, filling ratio and nanofluid concentration are considered. Plots are drawn between two input control parameters, at the same time; another two input control parameters remain constant as hold values. These hold values are cited in every surface and contour plots, in this work hold values take central values mentioned in Table 4.

3.1 Effects of operating parameters on wall temperature

Figure 10a, b shows that wall temperature is directly proportional to the power supply and it decreases with the rise in inclination angle up to 60° (approximately) and after that, it increases. Figure 10a shows that the wall temperature variations with a change in power supply and inclination angle (the FR and concentration of NF remained constant). Figure 10a shows that the wall temperature increases (the maximum increment is 20 °C) with power supply (50–150 W). When heat supply increases at the evaporator section, more heat is conducted through the wall surface in the axial direction and the radial direction. Heat absorption in radial direction depends upon various parameters like conductivity of wall surface and working fluid [30]. Heat is absorbed by working fluid conducted towards the condenser section. During movement of vapour from the evaporator section to the condenser section, heat is also conducted towards the wall surface of HP. It can be concluded that wall temperature will be higher for relatively less heat absorption and conduction through the working fluid. Therefore, the increase in heat supply to the evaporator section ultimately increases the wall temperature of HP. Figure 10b shows that wall temperature increases with the increase in power (50–150 W) supply at any inclination angle. Wall temperature decreases by 15 °C with the rise in inclination angle up to 60° (approximately) and beyond that it again increases. It is observed that the minimum temperature (less than 74 °C) occurs at 55 W power and 60° inclination angle (approximately). During the working of HP, the counter flow of vapour from the evaporator to condenser section and the condensate moving from condenser section to evaporator section interacts with each other and with other parts of HP also. During the interaction, heat exchange and fluid dynamics combine and show various outcomes. Buoyancy forces act in the upward direction and behave as a driving force for the vapour form of the working fluid. In the inclined position of HP (between 0 and 90°), the condensate of working fluid is moving in downward direction under the action of gravity. Capillary forces in wire mesh are also working in the same direction. Surface wettability is the property to spread the liquid on the surface [31]. It is the combined effects of surface characteristics, thermophysical properties of the liquid, surface tension and contact angle (liquid–solid interface). So there are a large number of parameters involved in this process. The optimum inclination angle is the balancing point of all the relevant parameters [26].

Figure 10c displays the temperature variation with inclination angle and nanofluid concentration (power and filling ratio remained constant). With the advancement of the nanofluid concentration and inclination angle, temperature decreases by 10 °C, after that temperature increases. Figure 10d shows that minimum wall temperature (maximum heat conductance) achieved with inclination angle 60° (approximately) and 1% nanofluid concentration.

Heat conductance increases (wall temperature decreases by 10 °C) up to 1% concentration, due to the increase in thermal conductivity of NF. Other thermophysical properties like specific heat and thermal diffusivity improve and leading to significant enhancement in heat transfer from the evaporator section to the condenser section. Suspended nanoparticles deposit on wall and mesh wick surface and change the surface characteristics. Deposition of nanoparticles on mesh wick surface acts as a coating layer leading to the enhancement in effective thermal conductivity of the wick structure and finally enhance the heat transfer performance of HP [22]. Deposition of nanoparticles (up to a certain limit) improves the capillary force and after that, if deposition further exceeds, the capillary force decreases. The decrease in capillary force causes a decrease in condensate flow from condenser to the evaporator section. The deposition limit up to which capillary force increases and after which it decreases will depend upon other design parameters of mesh wick like material, dia of mesh wire, aperture and porosity etc. [12]. Figure 10e, f shows surface and contour plot showing the variation in wall temperature with power and concentration (inclination angle and filling ratio remained constant). The reason for the aforesaid variation has already been explained. Figure 10g, h shows surface and contour plot showing the variation in wall temperature with filling ratio and concentration (inclination angle and power remained constant). It can be noticed that wall temperature reduces (by 12 °C) with the increase in filling ratio. Increase in filling ratio increases the heat absorption at the evaporator section. Enhanced heat absorption by the working fluid causes a decrease in wall temperature. In the present study, filling ratio increases from 30 to 70%. As the filling ratio increases at a constant power supply, the wall temperature decreases but if input power supply increases for given

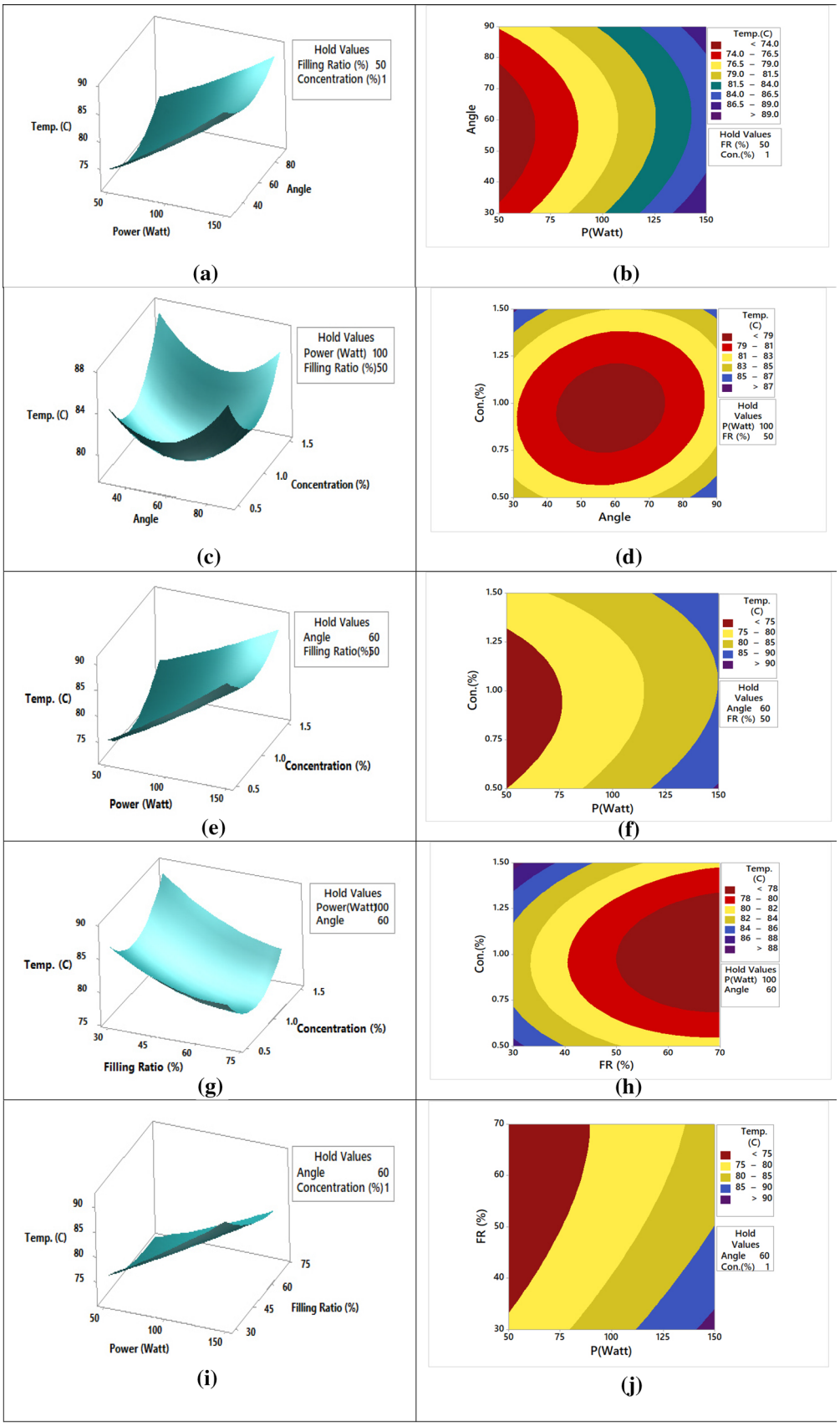
Hold Values
Filling Ratio (%) 50
Concentration (%) 1
Temp. (C)
Power (Watt)
Angle
(a)
Temp.(C)
< 74.0
74.0 – 76.5
76.5 – 79.0
79.0 – 81.5
81.5 – 84.0
84.0 – 86.5
86.5 – 89.0
> 89.0
Hold Values
FR (%) 50
Con.(%) 1
Angle
P(Watt)
(b)
Hold Values
Power (Watt) 100
Filling Ratio (%) 50
Temp. (C)
Concentration (%)
Angle
(c)
Temp. (C)
< 79
79 – 81
81 – 83
83 – 85
85 – 87
> 87
Hold Values
P(Watt) 100
FR (%) 50
Con.(%)
Angle
(d)
Hold Values
Angle 60
Filling Ratio (%) 50
Temp. (C)
Concentration (%)
Power (Watt)
(e)
Temp. (C)
< 75
75 – 80
80 – 85
85 – 90
> 90
Hold Values
Angle 60
FR (%) 50
Con.(%)
P(Watt)
(f)
Hold Values
Power(Watt) 100
Angle 60
Temp. (C)
Concentration (%)
Filling Ratio (%)
(g)
Temp. (C)
< 78
78 – 80
80 – 82
82 – 84
84 – 86
86 – 88
> 88
Hold Values
P(Watt) 100
Angle 60
Con.(%)
FR (%)
(h)
Hold Values
Angle 60
Concentration (%) 1
Temp. (C)
Filling Ratio (%)
Power (Watt)
(i)
Temp. (C)
< 75
75 – 80
80 – 85
85 – 90
> 90
Hold Values
Angle 60
Con.(%) 1
FR (%)
P(Watt)
(j)

◂**Fig. 10** Surface and contour plots of wall temperature with angle and power (**a**, **b**), with concentration and angle (**c**, **d**), with concentration and power (**e**, **f**), with concentration and filling ratio (**g**, **h**) and with filling ratio and power (**i**, **j**), respectively

filling ratio, the vapour pressure increases. If the increase in vapour pressure continues, the condition of vapour lock may occur. Figure 10i, j shows surface and contour plot showing the variation in wall temperature with power and filling ratio (inclination angle and nanofluid concentration remained constant). The reasons for the change in wall temperature with the increase in power and filling ratio have already been explained.

3.2 Effects of operating parameters on thermal resistance

During the experiments, water evaporates and moves towards the condenser section. Therefore, the concentration of NFs increased in the evaporator section. After condensation, water retuned back towards the evaporator section due to the capillary action. The movement of nanoparticles with water vapour, from the evaporator to condenser section, is not accepted by the majority of the researchers. Similarly, from the condenser to evaporator, water is raised due to the capillary action of mesh wick. Nanoparticles accumulated at the surface of the mesh and HP. Due to deposition of nanoparticles on the surface of the HP and mesh, an artificial porous layer is formed. There are bubbles formations at the solid–liquid interface. These bubbles are responsible for the TRHP. The nanoparticles punctured the bubbles and reduced the thermal resistance. Accumulation of nanoparticles on the wick surface builds an artificial porous layer which increases the capillary effect and thermal conductivity of the wick surface leading to the enhanced TPHP [22].

Figure 11a–h shows the variation in TRHP with the increase in all four operating parameters. The TRHP is calculated by Eqs. 4–6. The total thermal TRHP is the summation of evaporator thermal resistance and condenser thermal resistance. Figure 11a shows the variation in TR with the increase in power and inclination angle (FR and concentration of NF remained constant). From Fig. 11a, it can be noticed that the TRHP reduces with the increase in power (up to 120 W) after that it is increased slightly up to 150 W power. TR is reduced by 40% at 120 W power supply. The main reasons for change are like increase in TCNF, vapour velocity, micro-convection currents and critical heat flux [21]. As the power increases, the excess temperature (difference of solid surface and saturation temperature of liquid) increases. The bubbles movement from nucleation sites to the liquid surface is also increased. After reaching a certain value of excess temperature, the bubbles start collapsing and diffusing in the liquid and finally heat transfer takes place. Therefore, the increase in power supply reduces TRHP. Figure 11b shows the contour plot between the power and inclination angle, it was observed that minimum TR (less than 0.4 °C/W) occurs at 125 W power and 60° inclination angle (approximately). It can also be noticed that TR reduces (up to 40%) for 60° inclination angle and beyond that, it increases. There are two types of orientation (inclination angle) of HP, i.e., gravity-assisted and gravity opposes angles. In the present study, the authors considered gravity-assisted angles only. In gravity-assisted inclinations, condenser remains at a higher elevation as compared to the evaporator. So condensate flows in downward direction under the action of gravity. The capillary force also acts in the same direction (downward). The surface roughness of the wick and wall surface resists the condensate flow. Therefore, most favourable angle for the TPHP is the balancing point of all the above forces [32]. The wettability of solid surface depends upon the solid–liquid contact angle, surface temperature, inclination angle and thermophysical properties of the working fluid. The reason for the variation in TR with the change in power, filling ratio, nanofluid concentration and orientation of HP is almost similar as in the case of wall temperatures. Figure 11c displays the TR behaviour with inclination angle and concentration (power and filling ratio are constant). The effects of inclination angle on thermal resistance have been already explained. Figure 11d shows that minimum TR (less than 0.4 °C/W) noticed with the inclination angle of 60° and nanofluid concentration of 1.1%.

The TR of the evaporator section decreases with the increase in the concentration of NF. The possible mechanisms are due to the enhancement in TCNF, wettability, surface area and critical heat flux etc. [33]. Conversely, the TR of the condenser section increases with the increase in the concentration of NF. It is due to the increase in deposition of nanoparticles on the condenser surface. The reduction in thermal resistance at the evaporator section is higher as compared to the enhancement in thermal resistance of condenser section [29]. The total thermal resistance of HP is the summation of evaporator and condenser thermal resistances. Therefore, the overall TRHP decreases with the increase in the concentration of NFs.

Figure 11e, f shows the variation in TR with the increase in power and concentration. The reduction in TR is obtained by 50% for approximately 1.0% concentration and 120 W power supply. Mechanisms of variation in TR with the rise in power and concentration have been already explained. Figure 11g, h shows the variation in TR with the increase in concentration and FR. The reduction in TR is obtained by 50% for approximately 1.1% concentration and 50% FR. Similarly, the mechanisms/causes responsible for this variation have been discussed.

Figure 11i, j shows that minimum TR lies in filling ratio range of 43–58% (approximately) and a power range

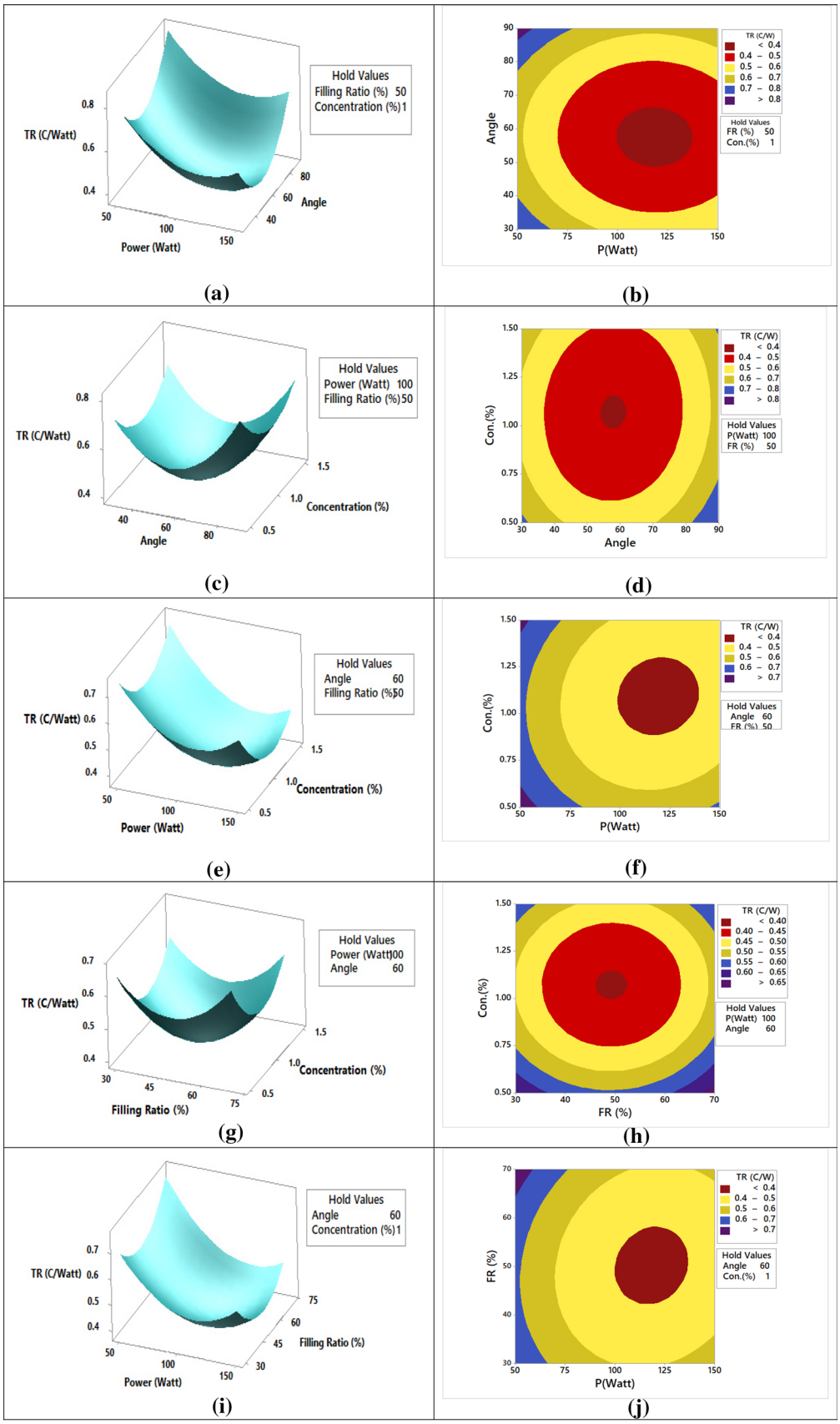
Hold Values
Filling Ratio (%) 50
Concentration (%) 1
TR (C/Watt)
Power (Watt)
Angle
(a)
TR (C/W)
< 0.4
0.4 – 0.5
0.5 – 0.6
0.6 – 0.7
0.7 – 0.8
> 0.8
Hold Values
FR (%) 50
Con.(%) 1
Angle
P(Watt)
(b)
Hold Values
Power (Watt) 100
Filling Ratio (%) 50
TR (C/Watt)
Angle
Concentration (%)
(c)
TR (C/W)
< 0.4
0.4 – 0.5
0.5 – 0.6
0.6 – 0.7
0.7 – 0.8
> 0.8
Hold Values
P(Watt) 100
FR (%) 50
Con.(%)
Angle
(d)
Hold Values
Angle 60
Filling Ratio (%) 50
TR (C/Watt)
Power (Watt)
Concentration (%)
(e)
TR (C/W)
< 0.4
0.4 – 0.5
0.5 – 0.6
0.6 – 0.7
> 0.7
Hold Values
Angle 60
FR (%) 50
Con.(%)
P(Watt)
(f)
Hold Values
Power (Watt) 100
Angle 60
TR (C/Watt)
Filling Ratio (%)
Concentration (%)
(g)
TR (C/W)
< 0.40
0.40 – 0.45
0.45 – 0.50
0.50 – 0.55
0.55 – 0.60
0.60 – 0.65
> 0.65
Hold Values
P(Watt) 100
Angle 60
Con.(%)
FR (%)
(h)
Hold Values
Angle 60
Concentration (%) 1
TR (C/Watt)
Power (Watt)
Filling Ratio (%)
(i)
TR (C/W)
< 0.4
0.4 – 0.5
0.5 – 0.6
0.6 – 0.7
> 0.7
Hold Values
Angle 60
Con.(%) 1
FR (%)
P(Watt)
(j)

◂**Fig. 11** Surface and contour plots of thermal resistance with angle and power (**a**, **b**), with concentration and angle (**c**, **d**), with concentration and power (**e**, **f**), with concentration and filling ratio (**g**, **h**) and with filling ratio and power (**i**, **j**) respectively

of 100–135%. The maximum reduction in TR noticed was 50% (approximately). The change in TR due to variation in power supply, inclination angle, concentration and FR have been discussed. The mechanisms responsible for the variation in TEHP with the change in power supply, inclination, filling ratio and nanofluid concentration are very similar that of wall temperature and TRHP. The change in wall temperature is responsible for the change in TRHP and TEHP.

The responsible mechanisms can be summarized as follows:

- The most dominating parameter, responsible for the change in TP is the enhancement in thermophysical properties of NFs.
- The nanofluid application enhances the critical heat flux; therefore, the operating range of HP increases.
- Due to deposition of nanoparticles on wall/wick surface, contact angle for solid–liquid surface decreases, wettability increases, and therefore, thermal performance improves.
- Deposition of nanoparticles builds a porous artificial layer on a solid surface, reduced the bubble formation rate and TRHP
- The most favourable inclination angle of HP exists at balancing point of the buoyancy force, gravitational force, viscous force and surface roughness etc.

These are the major and most accepted mechanism of enhanced heat transfer [30]. The research is still in the nascent stage. Therefore, it is inevitable to explore more facts to draw more firm conclusions.

3.3 Optimization response

RSM optimizer used to find optimum input parameters setting for best possible responses is shown in Fig. 12. The multi-objective optimization was carried with the different weightage of input parameters. The objective of the present study is to enhance the thermal efficiency (TE) with the lowest possible values of temperature and thermal resistance.

Optimum values of TE, TR and temperature were found 66.40%, 0.3884 °C/W and 78.86 °C with input parameters at 111.6 W Power, 58.5° inclination angle, 55% filling ratio and 1.1% concentration.

4 Test results validation

To validate the RSM best-utilized findings, experiments were carried out at 111.6 W Power, 58.5° inclination angle, 55% filling ratio and 1.1% concentration. The laboratory examination details are shown in Table 4 and shows the responses TE, TR and temperature. Experimental responses were compared with the RSM optimizer values (Table 6).

The percentage errors for the findings TE, TR and temperature are 2.86, 2.89 and 2.21, respectively, and were well within the limits. Hence, the RSM-predicted results can be applied for best utilize for the input setting. Kumaresan et al. [34] also examined the TPHP using CuO/H_2O NF as working fluid. Authors noticed the enhancement in TPHP using CuO/H_2O NF as the working fluid. Most favourable inclination angle and NF concentration was 60° and 1.0 vol%, respectively. Similarly, Venkatachalapathy et al. [35] also used CuO/H_2O NF as working fluid in HP. Researchers noticed a maximum reduction of 15.3 °C in evaporator wall temperature. Maximum reduction of 26.88% in TR was obtained at 60° inclination angle. It has been noticed that the experimental results of present work are in good agreement with the results of Kumaresan et al. [34] and Venkatachalapathy et al. [35].

4.1 Temporal deterioration in thermal performance

In prolonged working condition, due to sedimentation and agglomeration, the thermophysical properties of nanofluids deteriorate with time. Therefore, the thermal performance of nanofluid filled heat pipe also deteriorates. Figure 13 shows that the thermal efficiency of heat pipe deteriorates with time. In the present work, response surface methodology is used to optimize the thermal efficiency of the heat pipe. The optimum value of thermal efficiency was 64.54%. After the 1-week, thermal efficiency was 63.94%. The deterioration in thermal efficiency depends upon the nanofluid concentration. After 6 weeks, 4.2% deterioration in thermal efficiency was observed. The deterioration in thermal efficiency will depend upon nanoparticles type, size, concentration, base fluid etc.

Figure 14a, b shows the FE-SEM images of HP mesh surface before and after the application of NF.

It can be noticed that nanoparticles are deposited on the mesh surface after the experimentation. The change in surface characteristics depends upon shape, size and type of nanoparticles. There are many other hidden facts which decide the surface characteristics of the HP surface. The further study is required to explore the facts, related to the surface characterization of nanoparticle-deposited surface.

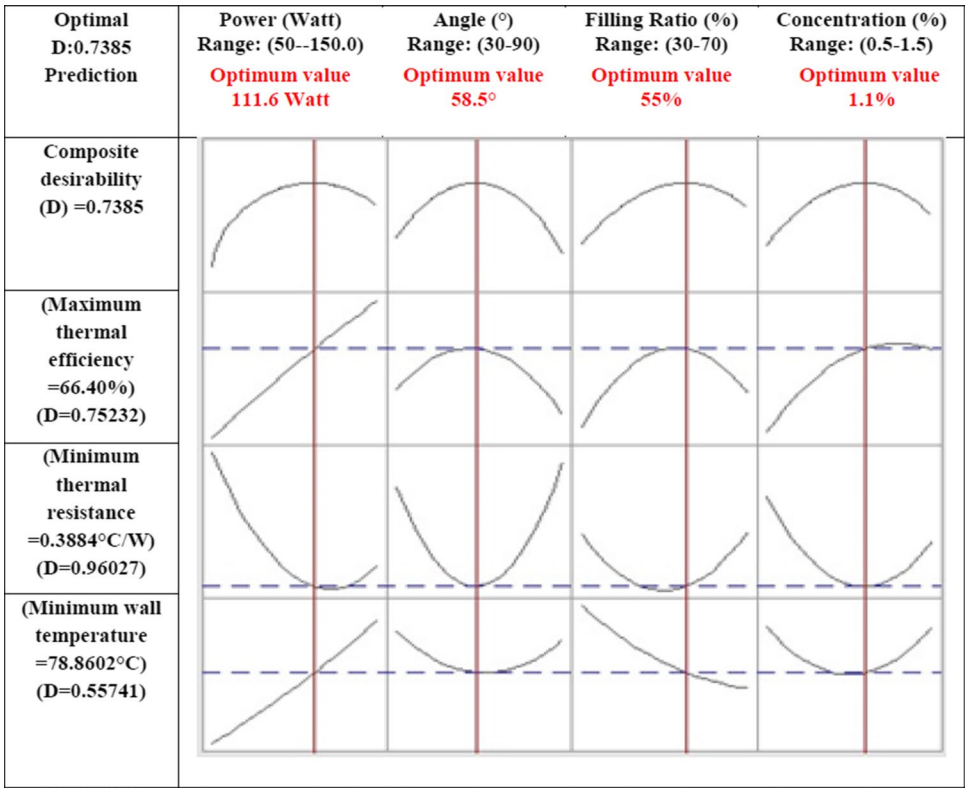

Fig. 12 Optimization plot

Table 6 Validation test

Response at 111.6 W, 58.5° inclination angle, 55% filling ratio and 1.1% concentration			
Response	Predicted	Actual	% Error
TE (%)	66.40	64.54	2.86
TR (°C/Watt)	0.3884	0.39996	2.89
Temperature (°C)	78.86	80.65	2.21

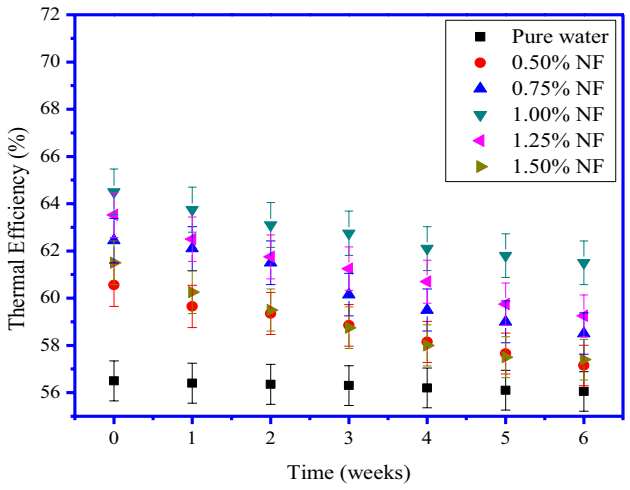

Fig. 13 Deterioration in the thermal efficiency of heat pipe with time

5 Conclusions

An experimental investigation was conducted for finding the thermal performance of heat pipe using CuO/H_2O nanofluids. Response surface methodology was used to predict the optimum value of thermal efficiency, thermal resistance and wall temperature of the heat pipe. A summary of the results obtained from the present investigation is presented below:

- CuO/H_2O nanofluid is an effective working fluid for the heat pipe. Thermal performance of heat pipe using CuO/H_2O nanofluids as working fluid is higher as compared to that of the base fluid.
- The optimum value of thermal efficiency, thermal resistance and wall temperatures are 66.4%, 0.3884 °C/W and 78.86 °C, respectively. Optimum values are obtained at 111.6 W power input, 55% filling ratio, 1.1% nanofluid concentration and 58.5° inclination angle.
- Response surface methodology is an effective tool to predict the thermal performance of the heat pipe in a wide range of operating parameters. The predicted and experimental data are in good agreement.

All operating and design parameters have their individual as well as combined effects on the thermal performance of heat pipes. More experimental and numerical studies are required to explore the interaction effect among all the

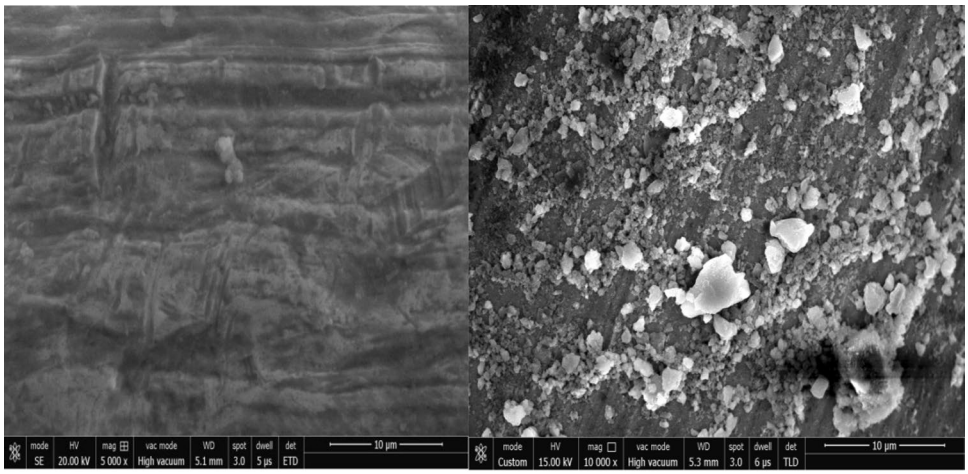

Fig. 14 FE-SEM images heat pipe mesh surface **a** before and **b** after the application of nanofluid

parameters of the heat pipe. Exploration of the hidden facts responsible for the change in thermal performance of heat pipe using various nanofluids is the future research work of the present study.

References

1. Choi SUS (1995) Enhancing thermal conductivity of fluids with nanoparticles. Proc 1995 ASME Int Mech Eng Congr Expo 231:99–105
2. Nasiri A, Shariaty-Niasar M, Rashidi AM, Khodafarin R (2012) Effect of CNT structures on thermal conductivity and stability of nanofluid. Int J Heat Mass Transf 55:1529–1535. https://doi.org/10.1016/j.ijheatmasstransfer.2011.11.004
3. Rathore PKS, Shukla SK, Gupta NK (2020) Synthesis and characterization of the paraffin/expanded perlite loaded with graphene nanoparticles as a thermal energy storage material in buildings. J Solar Energy Eng 142:1–8. https://doi.org/10.1115/1.4046087
4. Alam P, Gupta NK, Nizam AR (2020) Characterization of nanoparticles embedded phase change materials. Mater Today Proc. https://doi.org/10.1016/j.matpr.2020.02.606
5. Das SK, Putra N, Thiesen P, Roetzel W (2003) Temperature dependence of thermal conductivity enhancement for nanofluids. J Heat Transf 125:567. https://doi.org/10.1115/1.1571080
6. Trisaksri V, Wongwises S (2007) Critical review of heat transfer characteristics of nanofluids. Renew Sustain Energy Rev 11:512–523. https://doi.org/10.1016/j.rser.2005.01.010
7. Gupta NK, Mishra S, Tiwari AK, Ghosh SK (2019) A review of thermo physical properties of nanofluids. Mater Today Proc 18:968–978. https://doi.org/10.1016/j.matpr.2019.06.534
8. Das SK, Choi SUS, Patel HE (2006) Heat transfer in nanofluids—a review. Heat Transf Eng 27:3–19. https://doi.org/10.1080/01457630600904593
9. Murshed SMS, Leong KC, Yang C (2005) Enhanced thermal conductivity of TiO_2—water based nanofluids. Int J Therm Sci 44:367–373. https://doi.org/10.1016/j.ijthermalsci.2004.12.005
10. Alawi OA, Sidik NAC (2014) Influence of particle concentration and temperature on the thermophysical properties of CuO/R134a nanorefrigerant. Int Commun Heat Mass Transf 58:79–84. https://doi.org/10.1016/j.icheatmasstransfer.2014.08.038
11. Pang C, Jung J-Y, Lee JW, Kang YT (2012) Thermal conductivity measurement of methanol-based nanofluids with Al_2O_3 and SiO_2 nanoparticles. Int J Heat Mass Transf 55:5597–5602. https://doi.org/10.1016/j.ijheatmasstransfer.2012.05.048
12. Mahdavi M, Tiari S, De Schampheleire S, Qiu S (2018) Experimental study of the thermal characteristics of a heat pipe. Exp Therm Fluid Sci. https://doi.org/10.1016/j.expthermflusci.2018.01.003
13. Gupta NK, Tiwari AK, Ghosh SK (2018a) Heat transfer mechanisms in heat pipes using nanofluids—a review. Exp Therm Fluid Sci. https://doi.org/10.1016/j.expthermflusci.2017.08.013
14. Gupta NK, Verma SK, Kr P, Rathore S (2020) Effects of CuO/H_2O nanofluid application on thermal performance of mesh wick heat pipe. Heat Transf Res (Begell House). https://doi.org/10.1615/HeatTransRes.2020030772
15. Buschmann MH (2013) Nano fluids in thermosyphons and heat pipes: overview of recent experiments and modelling approaches. Int J Therm Sci 72:1–17. https://doi.org/10.1016/j.ijthermalsci.2013.04.024
16. Gupta NK, Tiwari AK, Ghosh SK (2018b) Experimental investigation of the thermal performance of mesh wick heat pipe. Heat Transf Res (Begell House) 49:1793–1811
17. Gupta NK, Tiwari AK, Ghosh SK (2018c) Experimental study of thermal performance of nanofluid-filled and nanoparticles-coated mesh wick heat pipes. J Heat Transf (Trans ASME) 140:1–7. https://doi.org/10.1115/1.4040146
18. Gupta NK, Tiwari AK, Verma SK, Rathore PKS, Ghosh SK (2019) A comparative study of thermal performance of a heat pipe using water and nanofluid, and a nanoparticle-coated wick heat pipe using water. Heat Transf Res 50(18):1767–1779
19. Gupta NK, Barua A, Mishra S, Singh SK, Tiwari AK, Ghosh SK (2019) Numerical Study of CeO_2/H_2O nanofluid application on thermal performance of heat pipe. Mater Today Proc 18:1006–1016. https://doi.org/10.1016/j.matpr.2019.06.541
20. Poplaski LM, Benn SP, Faghri A (2017) Thermal performance of heat pipes using nanofluids. Int J Heat Mass Transf 107:358–371. https://doi.org/10.1016/j.ijheatmasstransfer.2016.10.111
21. Solomon AB, Ramachandran K, Asirvatham LG, Pillai BC (2014) Numerical analysis of a screen mesh wick heat pipe with Cu/water nanofluid. Int J Heat Mass Transf 75:523–533. https://doi.org/10.1016/j.ijheatmasstransfer.2014.04.007
22. Huminic G, Huminic A (2013) Numerical study on heat transfer characteristics of thermosyphon heat pipes using nanofluids. Energy Convers Manag 76:393–399. https://doi.org/10.1016/j.enconman.2013.07.026

23. Mashaei PR, Shahryari M, Fazeli H, Hosseinalipour SM (2016) Numerical simulation of nanofluid application in a horizontal mesh heat pipe with multiple heat sources: a smart fluid for high efficiency thermal system. Appl Therm Eng 100:1016–1030. https://doi.org/10.1016/j.applthermaleng.2016.02.111
24. Mashaei PR, Shahryari M (2015) Effect of nanofluid on thermal performance of heat pipe with two evaporators; application to satellite equipment cooling. Acta Astronaut 111:345–355. https://doi.org/10.1016/j.actaastro.2015.02.003
25. Jafarmadar S, Azizinia N, Razmara N, Mobadersani F (2016) Thermal analysis and entropy generation of pulsating heat pipes using nanofluids. Appl Therm Eng 103:356–364. https://doi.org/10.1016/j.applthermaleng.2016.03.032
26. Senthilkumar R, Vaidyanathan S, Sivaraman B (2012) Effect of inclination angle in heat pipe performance using copper nanofluid. Procedia Eng 38:3715–3721. https://doi.org/10.1016/j.proeng.2012.06.427
27. Moffat RJ (1988) Describing the uncertainties in experimental results. Exp Therm Fluid Sci 1:3–17. https://doi.org/10.1016/0894-1777(88)90043-X
28. Wang P-Y, Chen X-J, Liu Z-H, Liu Y-P (2012) Application of nanofluid in an inclined mesh wicked heat pipes. Thermochim Acta 539:100–108. https://doi.org/10.1016/j.tca.2012.04.011
29. Solomon AB, Ramachandran K, Pillai BC (2012) Thermal performance of a heat pipe with nanoparticles coated wick. Appl Therm Eng 36:106–112. https://doi.org/10.1016/j.applthermaleng.2011.12.004
30. Ghanbarpour M, Nikkam N, Khodabandeh R, Toprak MS, Muhammed M (2015) Thermal performance of screen mesh heat pipe with Al_2O_3 nanofluid. Exp Therm Fluid Sci 66:213–220. https://doi.org/10.1016/j.expthermflusci.2015.03.024
31. Liu Z, Li Y, Bao R (2010) Thermal performance of inclined grooved heat pipes using nano fluids. Int J Therm Sci 49:1680–1687. https://doi.org/10.1016/j.ijthermalsci.2010.03.006
32. Putra N, Septiadi WN, Rahman H, Irwansyah R (2012) Thermal performance of screen mesh wick heat pipes with nanofluids. Exp Therm Fluid Sci 40:10–17. https://doi.org/10.1016/j.expthermflusci.2012.01.007
33. Gupta NK, Tiwari AK, Ghosh SK (2018d) Heat transfer mechanisms in heat pipes using nano fluids—a review. Exp Therm Fluid Sci 90:84–100. https://doi.org/10.1016/j.expthermflusci.2017.08.013
34. Kumaresan G, Venkatachalapathy S, Godson L, Wongwises S (2014) Comparative study on heat transfer characteristics of sintered and mesh wick heat pipes using CuO nano fluids ☆. Int Commun Heat Mass Transf 57:208–215. https://doi.org/10.1016/j.icheatmasstransfer.2014.08.001
35. Venkatachalapathy S, Kumaresan G, Suresh S (2015) Performance analysis of cylindrical heat pipe using nanofluids—an experimental study. Int J Multiph Flow 72:188–197. https://doi.org/10.1016/j.ijmultiphaseflow.2015.02.006